Applied Physics Letters

Mechanical signatures of degradation of the photovoltaic perovskite $CH_3NH_3PbI_3$ upon water vapor exposure

Cite as: Appl. Phys. Lett. **110**, 121903 (2017); https://doi.org/10.1063/1.4978687
Submitted: 07 February 2017 . Accepted: 26 February 2017 . Published Online: 20 March 2017

Massimo Spina, Ayat Karimi, Wanda Andreoni, Carlo A. Pignedoli, Bálint Náfrádi, László Forró, and Endre Horváth

Mechanical signatures of degradation of the photovoltaic perovskite $CH_3NH_3PbI_3$ upon water vapor exposure

Massimo Spina,[1] Ayat Karimi,[1] Wanda Andreoni,[2] Carlo A. Pignedoli,[3] Bálint Náfrádi,[1] László Forró,[1] and Endre Horváth[1]
[1]*Laboratory of Physics of Complex Matter, Ecole Polytechnique Fédérale de Lausanne, 1015 Lausanne, Switzerland*
[2]*Institute of Physics, Ecole Polytechnique Fédérale de Lausanne, 1015 Lausanne, Switzerland*
[3]*Swiss Federal Laboratories for Materials Science and Technology (EMPA), 8600 Dübendorf, Switzerland*

(Received 7 February 2017; accepted 26 February 2017; published online 20 March 2017)

We report on the mechanical properties of $CH_3NH_3PbI_3$ photovoltaic perovskite measured by nanoindentation. The Young's modulus (E) of the pristine sample is 20.0 ± 1.5 GPa, while the hardness (H) is 1.0 ± 0.1 GPa. Upon extended exposure to water vapor, both quantities decrease dramatically and the sample changes color from silver-black to yellow. Calculations based on density functional theory support this trend in the mechanical response. Chemical treatment of the degraded crystal in methylammonium iodide solution recovers the color of the pristine sample and the values of E and H within 50%. *Published by AIP Publishing*. [http://dx.doi.org/10.1063/1.4978687]

Hybrid (inorganic-organic) perovskite photovoltaics have opened a new exciting route in high-performance solar-cell technologies.[1] From the earliest reports on methylammonium (MA) lead iodide ($CH_3NH_3PbI_3$ or $MAPbI_3$),[2–4] great progress has been made in the synthesis of $MAPbI_3$ and related compounds as well as in the cell fabrication, leading to conversion efficiencies exceeding 20%.[5] Simultaneous intense research has been devoted to characterize the optical and electronic properties of these new materials (see, e.g., Refs. 6–8), and, in particular, to determine their relation with the structure of the various perovskite modifications, their variation with temperature, and the role of the chemical composition. However several issues, including the origin of the high-performance itself, are still unclear.[9]

On the other hand, the implementation of the organometallic halide perovskites in practical applications is still hindered by several problems and primarily instability under various environmental conditions.[9–11] One of the main concerns is their extreme sensitivity to hydration in a humid environment.[12–20] For example, in Ref. 13, in an ambient of relative humidity (RH) of 60%, the photoelectric efficiency reduces by 20% after only 18 h.

Both optical and infrared spectroscopies, as well as diverse structural studies of $MAPbI_3$ thin films, have identified PbI_2 as the ultimate product of prolonged exposure to humid air. This decomposition is believed to take place either after desorption of methylamine (CH_3NH_2) and hydrogen iodide (HI)[13] or of methylammonium iodide (CH_3NH_3I)[19] or via formation of hydrated phases, with signatures reminiscent of the monohydrate ($CH_3NH_3PbI_3{\cdot}H_2O$)[18] or the dihydrate ($(CH_3NH_3)_4PbI_6{\cdot}2H_2O$).[15,16] Recently, specific changes in the chemical composition have been proposed, apt to reduce the tendency to incorporate water.[21] On the theoretical side, computer simulations[22–24] have mainly focused on the interaction of water (as a layer or single molecules) with the perovskite surfaces and the mechanism leading to water insertion into the bulk. Clearly, degradation induced by moisture deserves further investigation and several properties of the materials should be monitored so as to gain a comprehensive understanding.

In this paper, we present an investigation of the mechanical characteristics of $MAPbI_3$—to which relatively limited attention has so far been paid[25–27]—and, in particular, to their variation under exposure to humid environments. Indeed, given that future devices will be exposed to diverse external mechanical forces (shocks, bending), characterization of the mechanical properties is undoubtedly crucial, especially to move from prototype to real large-scale applications. High volume fabrication processes—like the roll-to-roll method—as well as environmental conditions and portable/flexible uses can induce cracks, plastic deformations, and delamination that can ultimately degrade the optoelectronic performances. Moreover, there is no clue on possible further detrimental effects introduced by water penetration into the material. To gain insight into this matter, we quantitatively characterized the local mechanical properties of $MAPbI_3$ by the nano-indentation technique in dry as well as humid conditions. An estimate of the variation of the elastic moduli induced by water insertion into the lattice was obtained with calculations based on density functional theory (DFT).

Single crystals were prepared by precipitation from a concentrated aqueous solution of hydriodic acid containing lead (II) acetate trihydrate and a respective amount of CH_3NH_2 solution.[28] A constant 55–42 °C temperature gradient was applied to the solution. Large rhombohedral-shape crystals with silver-grey facets were obtained after seven days. Crystals of typical sizes of 3–8 mm were glued with an araldite epoxy adhesive (not reacting with the $MAPbI_3$ specimen) on an alumina support (Figure 1(a)) and subjected to indentation measurements. In each of them, nine indentation tests were performed (using a pyramidal Berkovich-type indenter) on a flat surface of the crystal, perpendicular to the applied force (Figure 1(b)). The maximum displacement of every measurement was set to 1 μm. This penetration depth was confirmed by confocal microscopy analysis of every indent (Figure 1(c)). From the load-displacement curves,

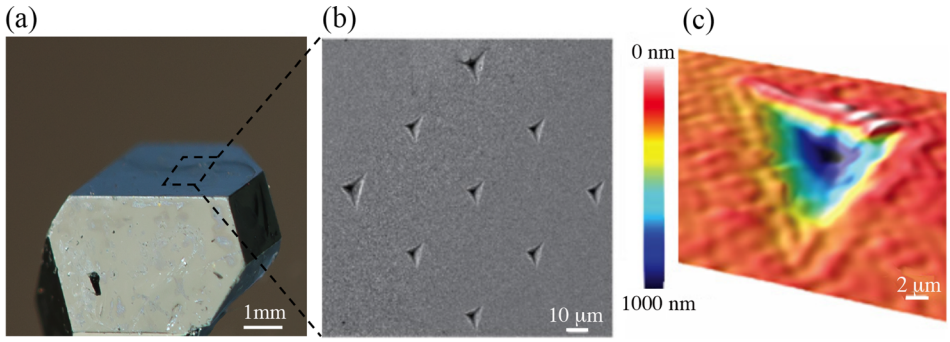

FIG. 1. (a) Optical image of a bulk single crystal of $MAPbI_3$; and (b) SE micrograph of the indentation tests effectuated on a flat crystal surface. (c) 3D confocal reconstruction of an indentation inprint.

using the Oliver-Pharr method,[29] both the Young's modulus E and the hardness H were extracted, as well as the energy of deformation.

In order to identify the consequences of water absorption on the mechanical properties, the crystal was kept in a normal laboratory environment of RH in the range 30%–50%, which corresponds to the operational conditions of $MAPbI_3$-based devices. Indentation measurements were performed at the following time points: at the beginning of the operation on the pristine (freshly prepared) sample and after 10, 60 (called aging stage 1), 70, 90, 163, and 170 (stage 2) days of aging.

For the freshly prepared $MAPbI_3$ crystal, in the tetragonal structure,[20] the mean values of the Young's modulus and the hardness are 20 ± 1.5 GPa and 1 ± 0.1 GPa, respectively. These data present a sizable discrepancy with two previous nano-indentation measurements on the tetragonal structure, namely, 10.7 (Ref. 25) or 14.3 GPa (Ref. 26) for the Young's modulus on the (100) face—with very slight dependence on the crystallographic orientation—and 0.25 (Ref. 25) or 0.5 GPa (Ref. 26) for the hardness. Based on the results discussed below, the origin of the discrepancy between these three sets of values might originate from difference in the crystal quality and age of the samples. For the sake of comparison, we notice that the results of analogous studies of PbI_2, using the nanoindentation method,[30] are approximately 17 GPa and 0.82 GPa for the elastic modulus and the hardness along the c-axis.

DFT calculations—using the Perdew-Burke-Ernzerhof (PBE) functional[31]—in Ref. 27 predict $E = 12.8$ GPa and $H = 0.54$ GPa (Ref. 31) for the tetragonal structure, $E = 15.0$ GPa and $H = 0.51$ GPa (Ref. 32) for the orthorhombic one, and more sizable variations for the pseudocubic modification ($E = 22.2$ GPa; $H = 0.98$ GPa (Ref. 32)). These values were derived from the elastic constants evaluated in the Voigt-Reuss-Hill approximation.[33,34] Our own results for the tetragonal structure, from analogous computations[35] and using the same exchange-correlation functional as in Ref. 27, are 16.7 GPa for E and 1.0 GPa for H. Beyond computational details, an important difference between the two calculations lies in the pseudopotentials, which include only scalar relativistic effects in Ref. 26 and also spin-orbit coupling in our scheme.[36]

When exposed to humid environment, we observed a gradual color change with time: from grayish/black—typical of the fresh crystal—to colorful interference patterns showing up after a few days in visible light, and eventually, after one or more months yellowish areas became clearly visible, indicating the presence of PbI_2.

Simultaneously, strong morphological modifications were clearly visible both in the optical microscope images (Figure 2(a)) and in the atomic force microcopy (AFM) maps (Figure 2(b)). The former showed spatially distinguishable surface structures extending over the entire crystal, whereas the latter revealed an increase in the local roughness of the surface with time. The surface roughness grew from 4 μm^2 in the pristine sample to 9 μm^2 of the stage 2 aged

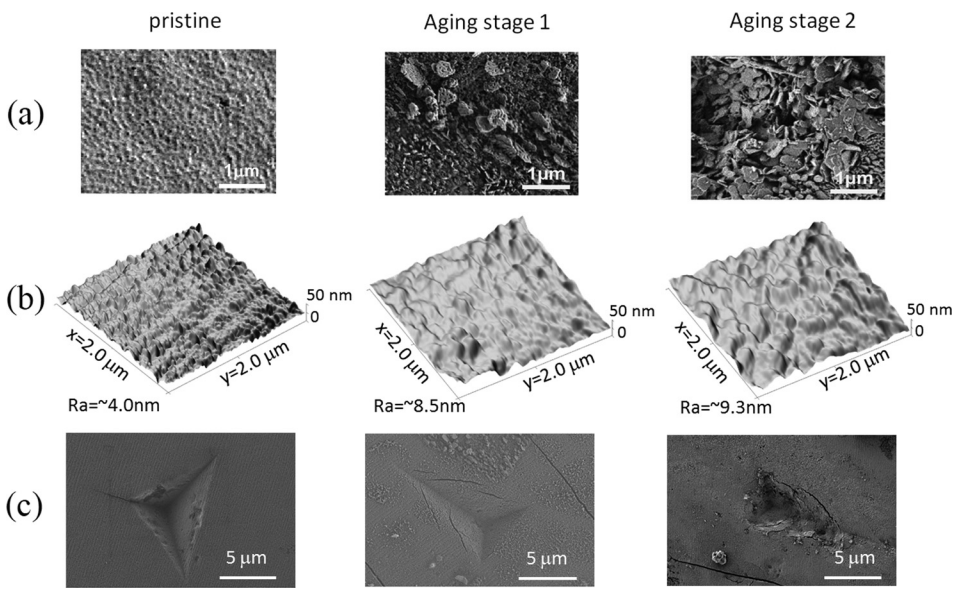

FIG. 2. Characterization of the crystal face and indent at three representative time points during water vapor exposure: pristine (freshly prepared crystal); aging stage 1 (exposed to 30%–50% RH for 60 days); and aging stage 2 (exposed to 30%–50% RH for 170 days). Row (a) Optical images; Row (b) 3D AFM reconstruction of the surface of the crystal with the mean roughness; and Row (c) SE micrographs of a representative indentation marks.

crystal. Eventually, cracks were revealed by the scanning electron microscopy (SEM) characterization of the indentation marks (Figure 2(c)). For the sake of comparison, we recall that in Ref. 16, uncoated thin films were observed to undergo a "smooth transformation to the byproducts," whereas the presence of cracks was detected for thin films coated with specific hole transport layers.

One can expect that morphological changes in the single crystal surfaces—here observed—translate into severe changes in the mechanical properties of the material. In particular, crack propagation can be seen as a sign of progressively reduced hardness of the material with increasing water incorporation.

Quantitative characterization of the mechanical response comes again from the load-displacement curves of indentation tests performed during the exposure of the material to humidity, at the time points mentioned above. An example is given in Figure 3. The behavior of the Young's modulus, hardness, and deformation energy as a function of time is derived from these curves measured at all time points. Figure 4 clearly shows that all these quantities decrease steadily and at a similar rate. In particular, we notice that both E and H fall to 20% of their pristine values in stage 2 aging, namely, after about 160 days.

It is interesting to note also that after 170 days the material was immersed in an oversaturated solution of methylammonium iodide in chloroform, apt to provide the evaporated components. Simultaneously, with the regeneration of the local structure of the pristine crystal—namely, with the exception of strongly damaged areas—and the reappearance of the silver-gray color, both E and H increased and could be recovered to ∼50% of their initial values. Otherwise, degradation would continue and the yellow color characteristic of the PbI_2 end product—although non-crystalline—becomes permanently dominant.

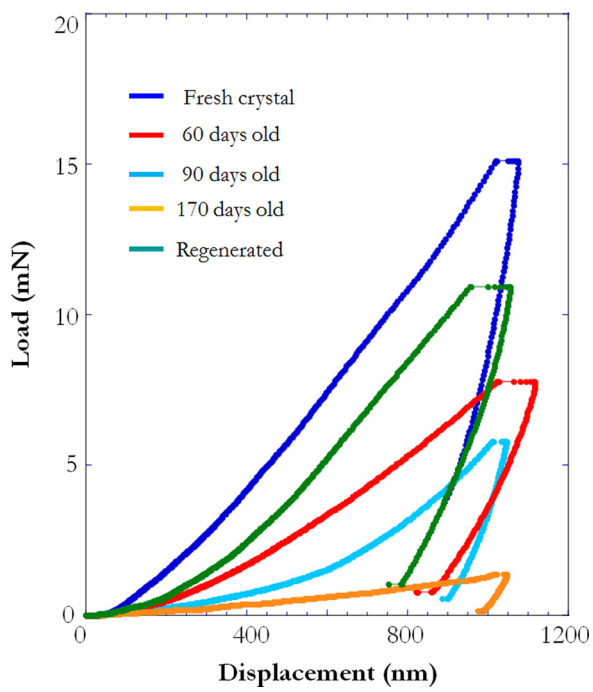

FIG. 3. Representative load-displacement curve of one indentation test performed at each step of the decomposition/regeneration cycle.

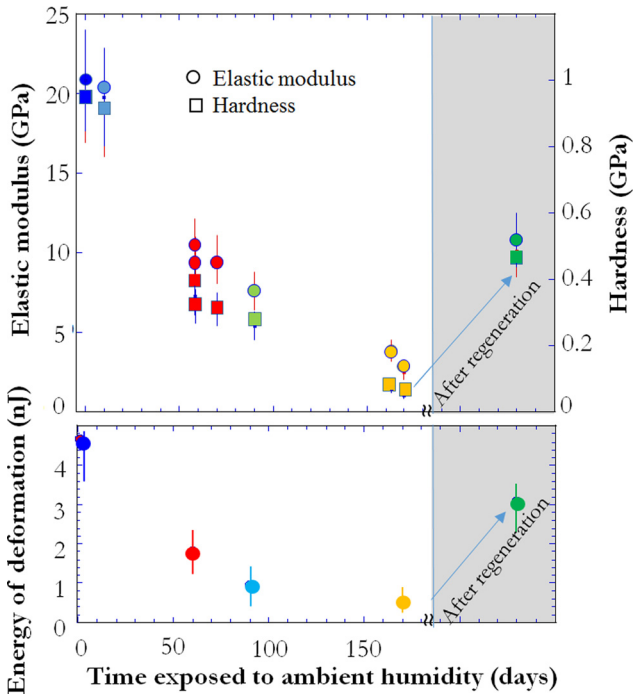

FIG. 4. Average values of the elastic (Young's) modulus, the hardness and the energy of deformation at each stage of the crystal degradation and after regeneration.

In order to gain some insights into the changes in the elastic moduli induced by water insertion in the tetragonal lattice of $MAPbI_3$ at the early stages, we have performed DFT calculations on (periodically repeated) cells with four molecular units as those of the dry samples. In this case, however, not only the optimization of the internal coordinates and cell parameters for the determination of the elastic constants but also a number of (uncorrelated) configurations so as to account—at least partially—for the orientational disorder of both methylammonium and water molecules are necessary. The initial configurations of the structural optimization runs were generated with DFT-molecular dynamics (MD) at 300–400 K. We verified that they were compatible with those observed in larger scale (periodically repeated) cells with additional (ultrashort) DFT-MD simulations run at the same temperature.

These models do not allow to simulate the destruction of the lattice, namely, the evaporation of given components and subsequent formation of holes in the structure, but permit to identify local deformations and especially can provide useful hints on the action of water.

Figure 5 illustrates two cases, one (Figure 5(a)) corresponding to one water molecule per MA (water concentration of 2.3%) and the other (Figure 5(b)) corresponding to 1.5 water molecules per MA (water concentration of 3.5%).

As expected, strong hydrogen bonds form between the water molecules and the ammonium ions (1.65–1.80 Å). These cause the tetragonal structure to transform into orthorhombic (with a ∼2% distortion) and to a decrease in the Young's modulus by ∼10%–15%. For increasing concentration, configurations with MA-water-MA and water-MA-water are observed (Figure 5(b)), and also with water-iodine hydrogen bonds (∼2.5 Å). The latter can indeed be considered as an indication of an incipient disruption of the local structure.

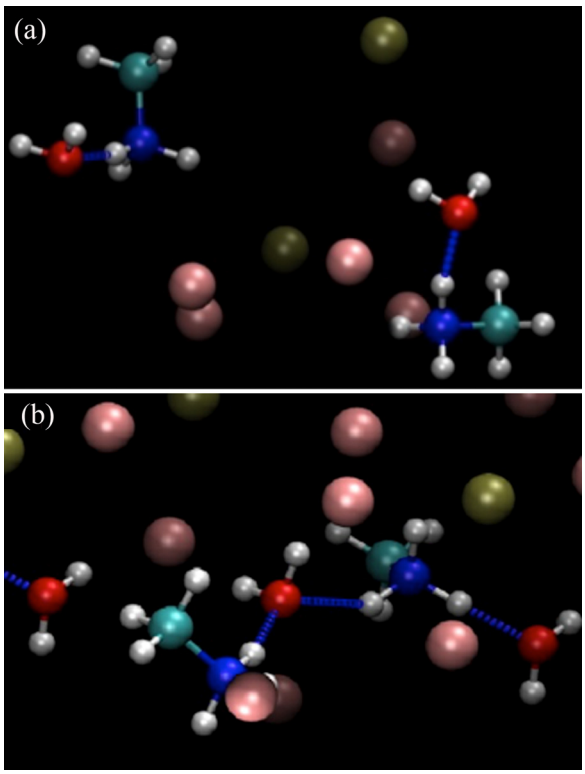

FIG. 5. Configurations of $MAPbI_3$ with water molecules at lower (a) and higher (b) concentrations. See text. Color code: silver (H), red (O), cyan (C), blue (N), green (Pb), and pink (I).

Correspondingly, although the distortion relative to a tetragonal structure is of the same order as for the lower concentration, the Young's modulus reduces drastically, namely, by about 70%. Values of the hardness of the material are more delicate to obtain. Still, a substantial decrease is found, of the same order as that of the Young's modulus. However, we expect that the calculated effects of water incorporation on the elastic moduli are overestimated because the small size of the replicas here employed might impose an artificial constraint on the freedom of water molecules to diffuse through different layers. In order to improve the quantitative predictions, extensive simulations using larger unit cells are needed.

In summary, the degradation process of single crystals of $MAPbI_3$ exposed to an RH of 30%–50% was monitored on the month timescale by morphological and mechanical analysis. At the early stage of water absorption, the structure deformed locally, but at later stages, large extended defects were identified, likely due to the evaporation of CH_3NH_2 and water, which strongly weakened the material. A steady and similar decrease in Young's modulus and hardness was found with time, down to 10%–20% of their initial values after 160 days. This trend may lead to fracture (radial and parallel cracks to the indent) and could result in device failure. On the other hand, recrystallization into $MAPbI_3$ can be obtained by dipping the sample into a CH_3NH_3I-saturated solution. This procedure partially recovered the $CH_3NH_3PbI_3$ structure and also the mechanical properties of the material locally but could not heal the extended defects. Our results on the water-induced degradation of the material towards decomposition with PbI_2 as dominant final product are consistent with available information on thin films exposed to humidity.

Preliminary DFT calculations of the variation of the crystal structural characteristics and the elastic moduli with water content at the early stages of absorption indicate how the insertion of water molecules progressively weakens the MA-iodine interactions and this reflects on the decrease in both Young's modulus and hardness. Additional simulations at larger size and time scales are however needed—and currently ongoing—to account for the intrinsic dynamic disorder of the material and water.

In conclusion, the results we presented here on the variation of the hardness and Young's modulus of $MAPbI_3$ single crystals are unprecedented. Extension of analogous studies to thin films—based on indentation measurements—is clearly desirable and could be achieved although with caution. Indeed, given the strong dependence of the mechanical response on the sample quality, indentation could serve as an easy and rapid test of the stage of the hydration-induced degradation of the devices.

See supplementary material for details of the computational scheme.

W.A. and C.A.P. wish to thank Dr. Pasquale Pavone for very useful discussions and Dr. Andrea Dal Corso for providing us with information on the pseudopotentials and related tests. Computational work was made possible by a grant from the Swiss National Supercomputing Centre—CSCS under Project No. ID 626. The ERC Advanced Grant Picoprop supported the work at LPMC.

[1]T. Baikie, Y. Fang, J. M. Kadro, M. Schreyer, F. Wei, S. G. Mhaisalkar, M. Graetzel, and T. J. White, J. Mater. Chem. A **1**, 5628 (2013).
[2]A. Kojima, K. Teshima, Y. Shirai, and T. Miyasaka, J. Am. Chem. Soc. **131**, 6050 (2009).
[3]J.-H. Im, C. R. Lee, J. W. Lee, S. W. Park, and N. G. Park, Nanoscale **3**, 4088 (2011).
[4]M. M. Lee, J. Teuscher, T. Miyasaka, T. N. Murakami, and H. J. Snaith, Science **338**, 643 (2012).
[5]M. Saliba, T. Matsui, K. Domanski, J.-Y. Seo, A. Ummadisingu, S. M. Zakeeruddin, J.-P. Correa-Baena, W. R. Tress, A. Abate, A. Hagfeldt, and M. Grätzel, Science **354**, 206 (2016).
[6]E. Mosconi, P. Umari, and F. De Angelis, Phys. Chem. Chem. Phys. **18**, 27158 (2016).
[7]E. Mosconi, C. Quarti, and F. De Angelis, in *Unconventional Thin Film Photovoltaics*, Energy and Environment Series 16, edited by E. Da Como, F. De Angelis, H. Snaith, and A. Walker (The Royal Society of Chemistry, 2016), pp. 234–296.
[8]S. Meloni, G. Palermo, N. Ashari-Astani, M. Grätzel, and U. Roethlisberger, J. Mater. Chem. A **4**, 15997 (2016).
[9]M. Graetzel, Nat. Mater. **13**, 838 (2014).
[10]B. Conings, J. Drijkoningen, N. Gauquelin, A. Babayigit, J. D'Haen, L. D'Olieslaeger, A. Ethirajan, J. Verbeeck, J. Manca, E. Mosconi, F. De Angelis, and H.-G. Boyen, Adv. Energy Mater. **5**, 1500477 (2015).
[11]J. Yang and T. L. Kelly, Inorg. Chem. **56**, 92 (2017).
[12]Y. Jingbi, Y. Yang, Z. Hong, T.-B. Song, L. Meng, Y. Liu, C. Jiang, H. Zhou, W.-H. Chang, G. Li, and Y. Yang, Appl. Phys. Lett. **105**, 183902 (2014).
[13]G. D. Niu, W. Z. Li, F. Q. Meng, L. D. Wang, H. P. Dong, and Y. Qiu, J. Mater. Chem. A **2**, 705 (2014).
[14]A. M. A. Leguy, Y. Hu, M. Campoy-Quiles, M. I. Alonso, O. J. Weber, P. Azarhoosh, M. van Schilfgaarde, M. T. Weller, T. Bein, J. Nelson, P. Docampo, and P. R. F. Barnes, Chem. Mater. **27**, 3397 (2015).
[15]J. A. Christians, P. A. Miranda Herrera, and P. V. Kamat, J. Am. Chem. Soc. **137**, 1530 (2015).

[16]J. Yang, B. D. Siempelkamp, D. Liu, and T. L. Kelly, ACS Nano **9**, 1955 (2015).
[17]C. Muüller, T. Glaser, M. Plogmeyer, M. Sendner, S. Doüring, A. A. Bakulin, C. Brzuska, R. Scheer, M. S. Pshenichnikov, W. Kowalsky, A. Pucci, and R. Lovrinčić, Chem. Mater. **27**, 7835 (2015).
[18]J. Zhao, B. Cai, Z. Luo, Y. Dong, Y. Zhang, H. Xu, B. Hong, Y. Yang, L. Li, W. Zhang, and C. Gao, Sci. Rep. **6**, 21976 (2016).
[19]M. Shirayama, M. Kato, T. Miyadera, T. Sugita, T. Fujiseki, S. Hara, H. Kadowaki, D. Murata, M. Chikamatsu, and H. Fujiwara, J. Appl. Phys. **119**, 115501 (2016).
[20]A. Arakcheeva, D. Chernyshov, M. Spina, L. Forró, and E. Horváth, Acta Cryst. B **72**, 716 (2016).
[21]J.-W. Lee, D.-H. Kim, H.-S. Kim, S.-W. Seo, S. M. Cho, and N.-G. Park, Adv. Energy Mater. **5**, 1501310 (2015).
[22]L. Zhang and P. H.-L. Sit, J. Phys. Chem. C **119**, 22370 (2015).
[23]N. Z. Koocher, D. Saldana-Greco, F. Wang, S. Liu, and A. M. Rappe, J. Phys. Chem. Lett. **6**, 4371 (2015).
[24]E. Mosconi, J. M. Azpiroz, and F. De Angelis, Chem. Mater. **27**, 4885 (2015).
[25]S. Sun, Y. Fang, G. Kieslich, T. J. White, and A. K. Cheetham, J. Mater. Chem. A **3**, 18450 (2015).
[26]Y. Rakita, S. R. Cohen, N. K. Kedem, G. Hodes, and D. Cahen, MRS Commun. **5**, 623 (2015).
[27]J. Feng, APL Mater. **2**, 081801 (2014).
[28]A. Poglitsch and D. Weber, J. Chem. Phys. **87**, 6373 (1987).
[29]W. C. Oliver and G. M. Pharr, J. Mater. Res. **19**, 3 (2004).
[30]W. Veiga and C. M. Lepienski, Mater. Sci. Eng., A **335**, 6 (2002).
[31]J. P. Perdew, K. Burke, and M. Ernzerhof, Phys. Rev. Lett. **77**, 3865 (1996); Erratum **80**, 891 (1998).
[32]H values are not reported in the original articles. We have derived them by using the relation H = (1–2 v), E/(6 (1 + v)) where E is the Young's modulus and v is Poisson's ratio.
[33]R. Hill, Proc. Phys. Soc. A **65**, 349 (1952).
[34]R. Hill, J. Mech. Phys. Solids **11**, 357 (1963).
[35]We use the ElaStic tool introduced in: R. Golesorkhtabar, P. Pavone, J. Spitaler, P. Puschnig, and C. Draxl, Comput. Phys. Commun. **184**, 1861 (2013).
[36]Our calculations use the relativistic soft pseudopotentials introduced in: A. Dal Corso and A. Mosca Conte, Phys. Rev. B **71**, 115106 (2005).